Oxygen vacancy control of electrical, optical, and magnetic properties of $Fe_{0.05}Ti_{0.95}O_2$ epitaxial films

Qing-Tao Xia(夏清涛) , Zhao-Hui Li(李召辉) , Le-Qing Zhang(张乐清), Feng-Ling Zhang(张凤玲), Xiang-Kun Li(李祥琨), Heng-Jun Liu(刘恒均), Fang-Chao Gu(顾方超), Tao Zhang(张涛), QiangLi(李强) , and Qing-Hao Li(李庆浩)
Citation: Chin. Phys. B, 2021, 30 (**11**): 117701. DOI: 10.1088/1674-1056/ac078e
Journal homepage: http://cpb.iphy.ac.cn; http://iopscience.iop.org/cpb

What follows is a list of articles you may be interested in

Irradiation behavior and recovery effect of ferroelectric properties of PZT thin films

Yu Zhao(赵瑜), Wen-Yue Zhao(赵文悦), Dan-Dan Ju(琚丹丹), Yue-Yue Yao(姚月月), Hao Wang(王豪), Cheng-Yue Sun(孙承月), Ya-Zhou Peng(彭亚洲), Yi-Yong Wu(吴宜勇), and Wei-Dong Fei(费维栋)
Chin. Phys. B, 2021, 30 (**10**): 107702. DOI: 10.1088/1674-1056/ac0dad

Recent advances, perspectives, and challenges inferroelectric synapses

Bo-Bo Tian(田博博), Ni Zhong(钟妮), Chun-Gang Duan(段纯刚)
Chin. Phys. B, 2020, 29 (**9**): 097701. DOI: 10.1088/1674-1056/aba603

Depolarization field in relaxor-based ferroelectric single crystals under one-cycle bipolar pulse drive

Chuan-Wen Chen(陈传文), Yang Xiang(项阳), Li-Guo Tang(汤立国), Lian Cui(崔莲), Bao-Qing Lin(林宝卿), Wei-Dong Du(杜伟东), Wen-Wu Cao(曹文武)
Chin. Phys. B, 2019, 28 (**12**): 127702. DOI: 10.1088/1674-1056/ab4e85

Hysteresis loop behaviors of ferroelectric thin films: A Monte Carlo simulation study

C. M. Bedoya-Hincapié, H. H. Ortiz-Álvarez, E. Restrepo-Parra, J. J. Olaya-Flórez, J. E. Alfonso
Chin. Phys. B, 2015, 24 (**11**): 117701. DOI: 10.1088/1674-1056/24/11/117701

Nanoscale domain switching mechanism of $Bi_{3.15}Eu_{0.85}Ti_3O_{12}$ thin film under the different mechanical forces

Zhu Zhe, Chen Yu-Bo, Zheng Xue-Jun
Chin. Phys. B, 2015, 24 (**10**): 107702. DOI: 10.1088/1674-1056/24/10/107702

Oxygen vacancy control of electrical, optical, and magnetic properties of $Fe_{0.05}Ti_{0.95}O_2$ epitaxial films*

Qing-Tao Xia(夏清涛)†, Zhao-Hui Li(李召辉)†, Le-Qing Zhang(张乐清), Feng-Ling Zhang(张凤玲), Xiang-Kun Li(李祥琨), Heng-Jun Liu(刘恒均), Fang-Chao Gu(顾方超), Tao Zhang(张涛), Qiang Li(李强)‡, and Qing-Hao Li(李庆浩)§

College of Physics, University-Industry Joint Center for Ocean Observation and Broadband Communication, Qingdao University, Qingdao 266071, *China*

(Received 20 February 2021; revised manuscript received 24 March 2021; accepted manuscript online 3 June 2021)

High-quality Fe-doped TiO_2 films are epitaxially grown on MgF_2 substrates by pulsed laser deposition. The x-ray diffraction and Raman spectra prove that they are of pure rutile phase. High-resolution transmission electron microscopy (TEM) further demonstrates that the epitaxial relationship between rutile-phased TiO_2 and MgF_2 substrates is 110 TiO_2 ‖ 110 MgF_2. The room temperature ferromagnetism is detected by alternative gradient magnetometer. By increasing the ambient oxygen pressure, magnetization shows that it decreases monotonically while absorption edge shows a red shift. The transport property measurement demonstrates a strong correlation between magnetization and carrier concentration. The influence of ambient oxygen pressure on magnetization can be well explained by a modified bound magnetization polarization model.

Keywords: ferromagnetic materials, semiconductors, epitaxial films, rutile TiO_2

PACS: 77.80.Dj, 78.40.Fy, 77.55.Px **DOI:** 10.1088/1674-1056/ac078e

1. Introduction

Dilute magnetic semiconductors (DMSs) have been extensively studied in the past decades, because they provide a promising method to inject spin polarized carriers into non-magnetic semiconductors.[1–11] The strong interaction between carriers and transition metal dopants enables synergetic use of both charge and spin degrees of freedom in one substance, which provides potential applications in spin-dependent electronics.[12–19] However, practical spintronic devices require DMS to have high Curie temperature (above room temperature (RT)), high spin polarization, intrinsic ferromagnetic origin and compatibility with semiconductor techniques. In order to realize RT DMS, various wide band gap oxides and nitrides have been extensively studied[20–32] based on the theoretical prediction by Dietl.[33] Particularly, 3d transition-metal-doped TiO_2 has been considered as one of the most promising candidates, for it possesses RT ferromagnetism, excellent transparency, stability, high n-type carrier mobility and low cost.[27,32–35]

Since the discovery of RT ferromagnetism in Co-doped TiO_2,[34] large numbers of studies of TiO_2-based DMS have been performed so far.[2,27,36,37] RT ferromagnetism has been reported in 3d transition-metal-doped TiO_2 in rutile, anatase and even amorphous phase; however, the origin of ferromagnetism remains controversial.[2,37,38] While most of researches support the intrinsic nature of ferromagnetism (FM) mediated by carriers or defects, some reports claimed that the segregation and formation of transition metal clusters or defects contribute to the FM signal.[39] In order to investigate fundamental properties and clarify inner mechanism of magnetic coupling, single crystal Fe:TiO_2 thin films are more favorable for the research. However, in the deposited thin films, the effects of lattice mismatch strain and interfacial dislocation between thin film and the substrate play an important role in determining the crystallinity, microstructure, and physics properties. Up to now, most of studies on TiO_2-based DMS have been performed on Si, MgO, $LaAlO_3$, $SrTiO_3$, or Al_2O_3 substrates;[36,40–43] either tensile strain or compressive strain can be introduced into the thin film, depending on lattice mismatch type. Notably, the strain effect can be utilized to tailor or optimize the properties of DMS thin films and help understand the interaction mechanism between charge carriers and magnetic impurity ions, even though a systematic and thorough understanding of strain effect is still unavailable and challenging.[41,42]

Rutile MgF_2 ($a = 4.62$ Å, $b = 4.62$ Å, $c = 3.051$ Å) has the same crystal structure as quite small lattice mismatch with rutile TiO_2 ($a = 4.593$ Å, $b = 4.593$ Å, $c = 2.959$ Å), as a result, MgF_2 is expected to be a most appropriate substrate for the epitaxial growth of rutile TiO_2, which has been seldom utilized.[44] In this work, high-quality thin films of 5% Fe-doped rutile TiO_2 were epitaxially grown on MgF_2 substrates

*Project supported by the National Natural Science Foundation of China (Grant No. 11504192) and the Natural Science Foundation of Shandong Province, China (Grant Nos. ZR201910230017 and BSB2014010).

†These authors contributed to this work equally.

‡Corresponding author. E-mail: liqiang@qdu.edu.cn

§Corresponding author. E-mail: qhli@qdu.edu.cn

by the pulsed laser deposition (PLD). The structural, optical, magnetic and transport properties of deposited films were investigated systematically. Structural analyses obtained from x-ray diffraction (XRD), Raman spectra, and transmission electron microscopy (TEM) proved that they are pure rutile phase epitaxial films of TiO_2, and had no impurity clusters detected. The UV-visible (UV-vis) transmittance study is characterized to infer the substitution of Fe in TiO_2 lattice corresponding to the band gap shift. The RT ferromagnetism and the variation in magnetization with deposition oxygen pressure are characterized by alternative gradient magnetometer (AGM). The RT FM and its oxygen pressure dependence is discussed with reference to the role of oxygen vacancy doping in TiO_2 lattice. These experimental results indicated that the oxygen vacancy doping concentration has a great influence on the FM behavior and band gap shift. This work demonstrates the potential applications of Fe-doped TiO_2 on MgF_2 substrates.

2. Materials and methods

The stoichiometric target was synthesized by standard solid state reaction of high-purity Fe_2O_3 and TiO_2 (99.99%) powders. The well ground powder was compressed into pellet with a radius of 4 cm and a thickness of 1 cm. Then the target was sintered at 1300 °C for 10 h. Considering the solubility limit of transition metal elements in TiO_2 lattice structure, here the magnetic dopant ion concentration was selected to be 5%, thus making the target a stoichiometric material $Fe_{0.05}Ti_{0.95}O_2$. The Ablation of the ceramic target was carried out using a KrF excimer laser ($\lambda = 248$ nm) with 300-mJ pulse at a repetition rate of 2 Hz.[36,43] Prior to the deposition, the MgF_2 substrate was ultrasonically cleaned in acetone and rinsed in ethanol. The temperature during growth of the films was maintained to be at 600 °C while the atmosphere varied under poor oxygen condition (5.0×10^{-5} Pa, 9.0×10^{-5} Pa, 1.4×10^{-4} Pa, and 3.0×10^{-4} Pa, denoted as Fe:TiO_2 (5.0×10^{-5} Pa), Fe:TiO_2 (9.0×10^{-5} Pa), Fe:TiO_2 (1.4×10^{-4} Pa), Fe:TiO_2 (3.0×10^{-4} Pa) respectively). Prior to film deposition, a buffer layer deposition of Fe:TiO_2 at 600 °C and 0.5 Pa was carried out to improve the crystallization of subsequent epitaxial layer. After the deposition, the samples were cooled down to room temperature under the same oxygen pressure as film growth.

The crystal structure of the obtained films was characterized by XRD (PG Instruments Ltd., Beijing, China) with Cu $K\alpha$ radiation ($\lambda = 0.15406$ nm) and Raman scattering spectra ranging from 100 cm^{-1} to 1000 cm^{-1} (NEXUS 670, Thermo Nicolet Co., USA). High-resolution transmission electron microscopy (HRTEM) and selected area electron diffraction (SAED) were employed to study the cross section microstructure of the interface with a Tecnai F30 transmission electron microscope operated at 300 kV. The optical transmittance measurements were performed using UV-vis spectrophotometer in a wavelength range from 200 nm to 800 nm (TU-1900, PG Instruments, Ltd.). The magnetic properties of the samples were measured by using an alternative gradient magnetometer (Micro Mag TM 2900, Prince-ton Measurement Corporation). Transport parameters (carrier concentration, resistivity and Hall mobility) were characterized by Hall effect with typical Van der Pauw configuration using a Keithley 2400 source meter. All the measurements were performed at room temperature.

3. Results and discussion

The θ–2θ XRD patterns of 5% Fe-doped TiO_2 epitaxial films on MgF_2 (110) substrates are shown in Fig. 1 in log scale. The XRD patterns reveal only peaks due to rutile TiO_2 as well as those due to MgF_2 substrate. The Fe-doped TiO_2 thin films are preferentially oriented in the (110) direction, in accordance with the (110) substrate utilized in this case. The inset in Fig. 1 shows the enlarged XRD pattern in the 2θ range of 56.1°–57.6°. The peak separation between TiO_2 (220) and MgF_2 (220) is about 0.16°. The full width at half maximum (FWHM) of TiO_2 (220) is about 0.12°, as highlighted in the inset of Fig. 1 from two-peak fitting, which is comparable to that of single crystal MgF_2 substrate with an FWHM value of about 0.15°. The high-quality crystallization of the thin film comes from the small lattice mismatch between MgF_2 substrate and rutile TiO_2.[39] The XRD pattern of MgF_2 substrate is also added for comparison, and neither secondary phase nor impurity forming is detected within the resolution limits of XRD, which implies the successful incorporation of substituting Fe cations into rutile TiO_2 lattice.

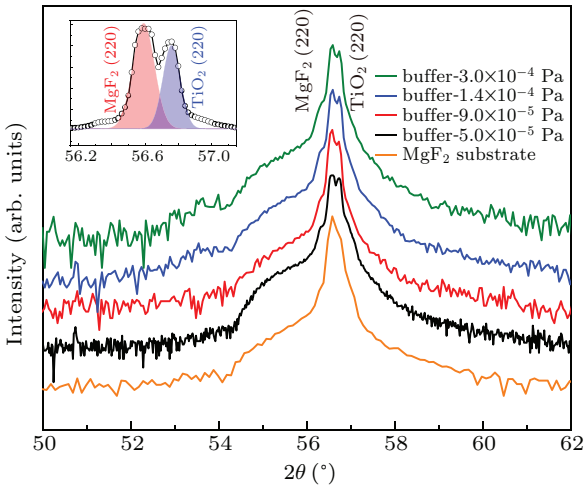

Fig. 1. XRD patterns of Fe:TiO_2 thin films deposited on MgF_2 substrates at various oxygen pressures, obtained by PLD (in log scale), with XRD pattern of MgF_2 substrate added here for comparison, and inset showing the enlarged region from 56.1° to 57.6° (in normal scale). Well separated MgF_2 (220) and TiO_2 (220) can be seen.

Raman spectrum is one of the most effective tools for the study of crystallinity, defects structure associated with the ma-

terials. Figure 2 presents the Raman spectra of Fe-doped TiO_2 thin films at various oxygen pressures in a range of 100 cm^{-1}–1000 cm^{-1}. Rutile is tetragonal and belongs to the space group ($P42/mnm$) with two TiO_2 molecules per unit cell. The first-order Raman spectrum of single crystal rutile TiO_2 shows four Raman active fundamental modes: B_{1g} (143 cm^{-1}), E_g (447 cm^{-1}), A_{1g} (612 cm^{-1}), and B_{2g} (826 cm^{-1}). Furthermore, the Raman spectra of rutile exhibit the intense second-order scattering feature.[45–47] In the Fe-doped TiO_2 thin film the main feature is the E_g mode and the A_{1g} mode, and the next feature is the second-order peaks centered at 241.5 cm^{-1} and 718.1 cm^{-1}. Note that the main feature of Fe-doped TiO_2 thin films is well consistent with that of pure rutile TiO_2 reference spectrum. In addition, two spiky peaks centered at about 297.8 cm^{-1} and 415.2 cm^{-1} can be attributed to MgF_2 substrate in our case, which can be well aligned with the reference spectrum of MgF_2 substrate. Reference spectra of pure hematite Fe_2O_3 and magnetite Fe_3O_4 are added in Fig. 2 for the peak alignment. These components are typical iron oxides, which may well emerge as secondary phases in the system. However, neither characteristic vibration modes of hematite Fe_2O_3 nor magnetite Fe_3O_4 can be found in the Raman spectra of Fe-doped TiO_2, which clearly indicates successful Fe incorporation into the host TiO_2 lattice instead of forming secondary phases.

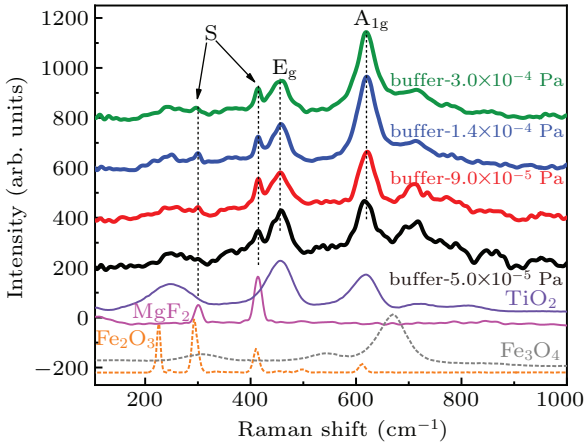

Fig. 2. Raman spectra of Fe:TiO_2 thin films deposited on MgF_2 substrates at various oxygen pressures, with e reference spectra of MgF_2 substrate, pure rutile TiO_2, hematite Fe_2O_3, and magnetite Fe_3O_4 added for detailed assign of each Raman peak.

Results from the cross sectional HRTEM image of Fe-doped TiO_2 film (1.4×10^{-4} Pa) near the interface region is shown in Fig. 3(a). The thin film has a thickness of around 30 nm and the incident electron beam is parallel to the [001] direction of the MgF_2 substrate and Fe-doped TiO_2 film. It is obvious that well-ordered single crystal film is epitaxially grown on the MgF_2 substrate oriented in the (110) direction, with an out-of-plane lattice parameter of 0.319 nm and an in-plane lattice parameter of 0.335 nm. The hetero interface between Fe-doped TiO_2 film and MgF_2 substrate indicated by arrows is indistinct.[44] Typical selected area electron diffraction pattern (SEAD) obtained from corresponding interface region is shown in Fig. 3(b). The fourfold symmetry reveals the tetragonal structure of TiO_2 and MgF_2. It is clear that there are no extra spots or splitting of reflections but only (001) zone axis pattern. Further analysis from the HRTEM and the SAED analysis indicate that the deposited thin film on MgF_2 substrate is of single crystalline rutile phase, with an epitaxial relationship of (110)[-110] TiO_2 ‖ (110)[-110] MgF_2, which originates from the small lattice mismatch between TiO_2 and MgF_2 substrate. These features confirm the high-quality and perfect epitaxy of Fe-doped TiO_2 thin film on MgF_2 substrate in the rutile phase, consistent with the XRD and Raman spectra.

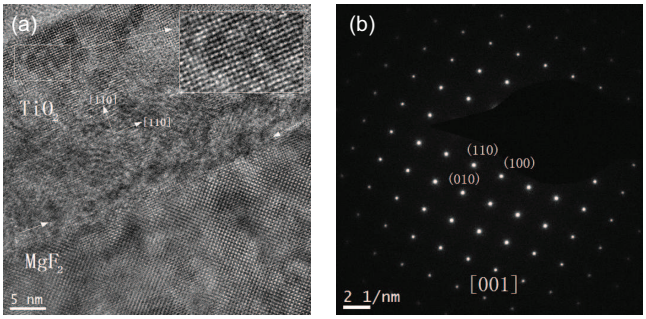

Fig. 3. (a) Cross section TEM image of interface between Fe:TiO_2 thin film and MgF_2 substrate viewed in the [001] direction; (b) selected area electron diffraction patterns for Fe-doped TiO_2 film on MgF_2 substrate.

Figure 4 shows the room temperature UV-vis transmittance spectra of Fe-doped TiO_2 thin films deposited at varying growth oxygen pressures. Note that MgF_2 substrate shows a large transmittance of above 95% in the region of 200 nm –600 nm, hence the spectra here present mostly the intrinsic features of the deposited DMS thin films. In general, all the films are well transparent in the visible light region from 200 nm to 600 nm in our case, with an average transmittance of about 50%. Strong light absorption appears at about 320 nm due to the transition from the valence band top to conduction band bottom. The corresponding optical band gap can be determined from absorption coefficient and photon energy[48–51] and can be directly visualized from the absorption edge shift. Note that with the increase of growth oxygen pressure, the absorption edge shifts to longer wavelength and the corresponding band gaps of all samples decrease monotonically. The narrowing of band gap with the increase of oxygen pressure has been previously reported in deposited TiO_2 thin films.[52,53] Such a red shift can be explained as being mainly due to the band shift from the shallow donor level of oxygen non-stoichiometry under lower oxygen pressure, meanwhile the slight crystallization evolution and parental lattice variation may play a significant part.[52,53]

The magnetic properties of Fe-doped TiO_2 thin films are investigated by using AGM at room temperature, with external

magnetic field being perpendicular to the film surface. Distinct ferromagnetic behaviors can be observed in all the films as shown in Fig. 5. Note that with the increase of deposition oxygen pressure, the saturation magnetization of thin film decreases monotonically from 25 emu/cm^3 to 7 emu/cm^3 as shown in the inset of Fig. 5. Considering a constant transition metal dopant concentration of 5% and the flourishing of oxygen vacancy under a lower growth oxygen pressure, the monotonic decrease of saturation magnetization implies the strong correlation between ferromagnetic coupling effect and the oxygen deficiency lattice.

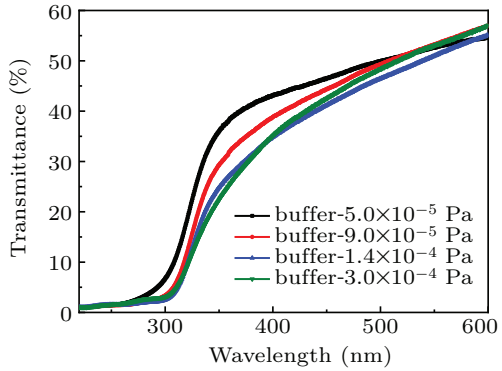

Fig. 4. Ultraviolet-visible transmittance spectra of epitaxial TiO_2 films deposited on MgF_2 substrates at different oxygen pressures, where absorption edge shows monotonic shift to larger wavelength with oxygen pressure increasing.

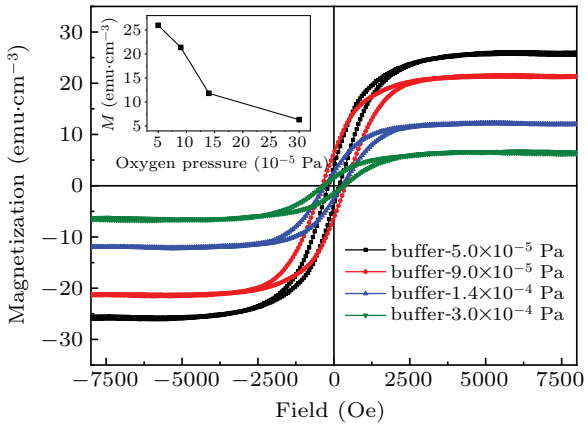

Fig. . Magnetic hysteresis loops of Fe-doped TiO_2 thin film on MgF_2 substrates at different growth oxygen pressures, where inset shows saturation magnetization of Fe-doped TiO_2 film at growth oxygen pressure. The unit 1 Oe = 79.5775 A·m^{-1}.

In order to clarify the origin of ferromagnetic property of Fe-doped TiO_2 thin film on MgF_2 substrate, Hall effect characterization is employed to study the transport properties of corresponding films. The results of film resistivity, carrier concentration and mobility are shown in Figs. 6(a)–6(c), respectively. Note that with the increase of growth oxygen pressure, film resistivity increases almost linearly from 0.1 Ω/cm to 4.6 Ω/cm, while the measured carrier concentration decreases significantly. Meanwhile the carrier mobility keeps almost constant, specifically it slightly increases with growth oxygen pressure rising. The low resistivity and high carrier concentration demonstrate the potential applications of the films in semiconductor devices.

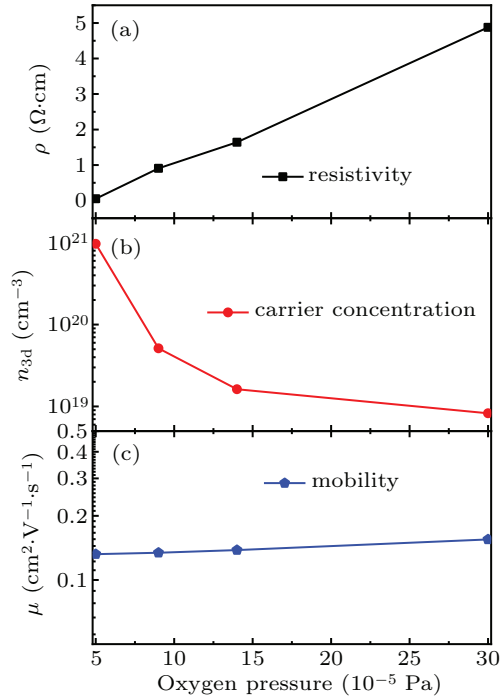

Fig. 6. Transport properties of Fe:TiO_2 thin film on MgF_2 substrate, showing variation of its (a) resistivity, (b) carrier concentration, and (c) mobility with oxygen pressure.

Considering the relatively low doping concentration of transition metal cations of 5%, which is far below the percolation threshold, traditional double exchange or super exchange model cannot explain the strong FM in this material. In the DMS system, bounded magnetic polaron (BMP) scenario is widely accepted to explain the FM.[54–56] The exchange interaction between localized magnetic cations and itinerant sp electrons, if it once percolates throughout the entire film, may well lead to the experimental detected macroscopic RT FM. Besides the magnetic properties, Chou *et al.* further proposed a modified BMP model to include the correlation between electric transport and magnetic properties in DMS.[57] The modified BMP model can be utilized to explain the magnetic coupling in this system. As the concentration of oxygen vacancies increases, the number of BMP spheres increases.. Meanwhile, the increase of carrier concentration also enlarges the radius of BMP sphere.[36] These correlated factors brings about the phenomenal FM string enhancement on Fe-doped TiO_2 film deposited on MgF_2 substrate with the decrease of growth oxygen pressure. In previous research, secondary phase formation has been proposed as another possible origin of RTFM in a typical DMS system.[40] Based on our structural characterizations, no foreign phase formation is detected to the resolution limit, particularly magnetic active hematite and magnetite phases can be excluded in Raman spectra. The correlation between oxygen pressure and optical, magnetic, transport properties further implies single phase

Fe-doped TiO_2 as the origin of intrinsic multifunctional properties. The integrating of multifunction properties into one system provides promising potential for future applications in multifunctional electronic devices.

4. Conclusions

In this work, 5%-Fe-doped TiO_2 thin films in rutile phase are epitaxially deposited on MgF_2 substrate by the PLD method. The small mismatch between rutile TiO_2 and MgF_2 substrate determines the high crystalline quality of DMS films, which is demonstrated by XRD, Raman spectra, and HRTEM. The deposition oxygen pressure plays an important role in determining the optical, transport, and magnetic properties. Optical band gap, carrier concentration, and magnetization can be well dependent on the oxygen deficiency atmosphere. The RT FM observed in all the DMS films shows that it is strongly correlated with the carrier concentration introduced by oxygen vacancy, which can be explained by a modified BMP model. This work demonstrates the high-quality Fe-doped TiO_2 DMS film deposited on MgF_2 substrate, which is required for potential applications in magneto–optical and magneto–electric devices, and also for fundamental study of DMS coupling mechanism.

References

[1] Dietl T 2010 *Nat. Mater.* **9** 965
[2] Prellier W, Fouchet A and Mercey B 2003 *J. Phys.: Condes. Matter.* **15** R1583
[3] Ando K 2006 *Science* **312** 1883
[4] Li Q, Qiao R, Mehta A, Lü W, Zhou T, Arenholz E, Wang C, Chen Y, Li L, Tian Y, Bai L, Hussain Z, Zheng R, Yang W and Yan S 2020 *Sci. Bull.* **65** 1718
[5] Zhang F, Zheng B, Sebastian A, Olson D H, Liu M, Fujisawa K, Pham Y T H, Jimenez V O, Kalappattil V, Miao L, Zhang T, Pendurthi R, Lei Y, Elías A L, Wang Y, Alem N, Hopkins P E, Das S, Crespi V H, Phan M H and Terrones M 2020 *Adv. Sci.* **7** 2001174
[6] Phan V N and Nguyen H N 2020 *Phys. Rev. B* **102** 125202
[7] Cai Y X, Zhang Y D, Dang B S, Wu H, Wang J F and Yuan P 2011 *Acta Phys. Sin.* **60** 040701 (in Chinese)
[8] Paul S, Dalal B, Das M, Mandal P and De S K 2019 *Chem. Mater.* **31** 8191
[9] Li Q, Shen T T, Dai Z K, Cao Y L, Yan S S, Kang S S, Dai Y Y, Chen Y X, Liu G L and Mei L M 2012 *Appl. Phys. Lett.* **101** 172405
[10] Li X L and Xu X H 2019 *Chin. Phys. B* **28** 098506
[11] Wei Z M and Xia J B. 2019 *Acta Phys. Sin.* **68** 163201 (in Chinese)
[12] Jean-Baptiste M 2013 *J. Phys. D: Appl. Phys.* **46** 143001
[13] Zhang K, Cao Y L, Fang Y W, Li Q, Zhang J, Duan C G, Yan S S, Tian Y F, Huang R, Zheng R K, Kang S S, Chen Y X, Liu G L and Mei L M 2015 *Nanoscale* **7** 6334
[14] Song C, Cui B, Li F, Zhou X and Pan F 2017 *Prog. Mater. Sci.* **87** 33
[15] Pham Y T H, Liu M, Jimenez V O, Yu Z, Kalappattil V, Zhang F, Wang K, Williams T, Terrones M and Phan M H 2020 *Adv. Mater.* **32** 2003607
[16] You J Y, Gu B, Maekawa S and Su G 2020 *Phys. Rev. B* **102** 094432
[17] Luo X, Zhang F, Li Q, Xia Q, Li Z, Li X, Ye W, Li S and Ge C 2020 *J. Phys.: Condes. Matter.* **32** 334001
[18] Guo S L and Ning F L 2018 *Chin. Phys. B* **27** 097502
[19] Long L, Yi P G, Chao Z H, Tao H L, Huang J T, Yu W Y, Chen R X, Lou M S and Yan L B 2020 *Chin. Phys. B* **29** 097102
[20] He M, Tian Y F, Springer D, Putra I A, Xing G Z, Chia E E M, Cheong S A and Wu T 2011 *Appl. Phys. Lett.* **99** 222511
[21] Hsu H S, Huang J C A, Huang Y H, Liao Y F, Lin M Z, Lee C H, Lee J F, Chen S F, Lai L Y and Liu C P 2006 *Appl. Phys. Lett.* **88** 242507
[22] Kim H, Osofsky M, Miller M M, Qadri S B, Auyeung R C Y and Piqué A 2012 *Appl. Phys. Lett.* **100** 032404
[23] Liu G L, Cao Q, Deng J X, Xing P F, Tian Y F, Chen Y X, Yan S S and Mei L M 2007 *Appl. Phys. Lett.* **90** 052504
[24] Tian Y, Li Y, He M, Putra I A, Peng H, Yao B, Cheong S A and Wu T 2011 *Appl. Phys. Lett.* **98** 162503
[25] Xing P F, Chen Y X, Yan S S, Liu G L, Mei L M, Wang K, Han X D and Zhang Z 2008 *Appl. Phys. Lett.* **92** 022513
[26] de Godoy M P F, Mesquita A, Avansi W, Neves P P, Chitta V A, Ferraz W B, Boselli M A, Sabioni A C S and de Carvalho H B 2013 *J. Alloys Compd.* **555** 315
[27] Kaushik A, Dalela B, Kumar S, Alvi P A and Dalela S 2013 *J. Alloys Compd.* **552** 274
[28] Philip J, Punnoose A, Kim B I, Reddy K M, Layne S, Holmes J O, Satpati B, LeClair P R, Santos T S and Moodera J S 2006 *Nat. Mater.* **5** 298
[29] Zhou T, Wei L, Xie Y, Li Q, Hu G, Chen Y, Yan S, Liu G, Mei L and Jiao J 2012 *Nanoscale Res. Lett.* **7** 1
[30] Zhu D, Liu G, Xiao S, Yan S, He S, Cai L, Li Q, Cao Q, Hu S, Chen Y, Kang S and Mei L 2013 *J. Appl. Phys.* **113** 173701
[31] Han R L and Yan Y 2018 *Chin. Phys. B* **27** 117505
[32] Xiao L L and Xiao H X. 2019 *Chin. Phys B* **28** 098506
[33] Dietl T, Ohno H, Matsukura F, Cibert J and Ferrand D 2000 *Science* **287** 1019
[34] Matsumoto Y, Murakami M, Shono T, Hasegawa T, Fukumura T, Kawasaki M, Ahmet P, Chikyow T, Koshihara S Y and Koinuma H 2001 *Science* **291** 854
[35] Yamada Y, Ueno K, Fukumura T, Yuan H T, Shimotani H, Iwasa Y, Gu L, Tsukimoto S, Ikuhara Y and Kawasaki M 2011 *Science* **332** 1065
[36] Li Q, Wei L, Xie Y, Jiang F, Zhou T, Hu G, Jiao J, Chen Y, Liu G, Yan S and Mei L 2013 *J. Alloys Compd.* **574** 67
[37] Xu N N, Li G P, Lin Q L, Liu H and Bao L M 2016 *Chin. Phys. B* **25** 116103
[38] Lee Y J, Jong M P D, Wiel W G V D, Kim Y and Brock J D 2010 *Appl. Phys. Lett.* **97** 212506
[39] Singhal R K, Samariya A, Kumar S, Xing Y T, Jain D C, Dolia S N, Deshpande U P, Shripathi T and Saitovitch E B 2010 *J. Appl. Phys.* **107** 113916
[40] Zhang Y, Qi Y Y, Hu Y H and Liang P 2013 *Chin. Phys. B* **22** 127101
[41] Nguyen H H, Prellier W, Sakai J and Ruyter A 2004 *J. Appl. Phys.* **95**
[42] Schuisky M, HRsta A, Aidla A, Kukli K, Kiisler A A and Aarik J 2000 *J. Electrochem. Soc.* **147** 3319
[43] Chen M C and Jiang A Q. 2011 *Chin. Phys. Lett.* **28** 077701
[44] Xie Y, Wei L, Li Q, Chen Y, Yan S, Jiao J, Liu G and Mei L 2016 *J. Alloys Compd.* **683** 439
[45] Aita C R 2007 *Appl. Phys. Lett.* **90** 213112
[46] Chen C A, Huang Y S, Chung W H, Tsai D S and Tiong K K 2009 *J. Mater. Sci.: Mater. Electron.* **20** 303
[47] Yang J Y, Ma H L, Ma G H, Lu B and Ma H 2007 *Appl. Phys. A* **88** 801
[48] Gupta R K, Ghosh K and Kahol P K 2010 *Mater. Lett.* **64** 2022
[49] Shinde V R, Gujar T P, Lokhande C D, Mane R S and Han S H 2006 *Mater. Chem. Phys.* **96** 326
[50] Singh J, Sharma S, Sharma S and Singh R C 2019 *Optik* **182** 538
[51] Mayabadi A H, Waman V S, Kamble M M, Ghosh S S, Gabhale B B, Rondiya S R, Rokade A V, Khadtare S S, Sathe V G, Pathan H M, Gosavi S W and Jadkar S R 2014 *J. Phys. Chem. Solids* **75** 182
[52] Tantray F A, Agrawal A, Gupta M, Andrews J T and Sen P 2016 *Thin Solid Films* **619** 86
[53] Horprathum M, Eiamchai P, Chindaudom P, Pokaipisit A and Limsuwan P 2012 *Procedia Engineering* **32** 676
[54] Kaminski A and Das Sarma S 2002 *Phys. Rev. Lett.* **88** 247202
[55] Coey J M D, Venkatesan M and Fitzgerald C B 2005 *Nat. Mater.* **4** 173
[56] Deepika, Kumar R, Kumar R, Yadav K P, Vaibhav P, Sharma S, Singh R K and Kumar S 2020 *Chin. Phys. B* **29** 108503
[57] Chou H, Lin C P, Huang J C A and Hsu H S 2008 *Phys. Rev. B* **77** 245210